PRIMARY RESEARCH ARTICLE

High ecosystem stability of evergreen broadleaf forests under severe droughts

Kun Huang[1,2] | Jianyang Xia[1,3]

[1]Zhejiang Tiantong Forest Ecosystem National Observation and Research Station, Shanghai Key Lab for Urban Ecological Processes and Eco-Restoration, School of Ecological and Environmental Sciences, East China Normal University, Shanghai, China

[2]Center for Global Change and Ecological Forecasting, East China Normal University, Shanghai, China

[3]Institute of Eco-Chongming, Shanghai, China

Correspondence
Jianyang Xia, Zhejiang Tiantong Forest Ecosystem National Observation and Research Station, Shanghai Key Lab for Urban Ecological Processes and Eco-Restoration, School of Ecological and Environmental Sciences, East China Normal University, Shanghai, China.
Email: jyxia@des.ecnu.edu.cn

Funding information
China Postdoctoral Science Foundation, Grant/Award Number: 2016M591627; Fok Ying Tong Education Foundation, Grant/Award Number: 161016; National Key R&D Program of China, Grant/Award Number: 2017YFA0604600; National Natural Science Foundation of China, Grant/Award Number: 31722009 and 41601099

Abstract

Global increase in drought occurrences threatens the stability of terrestrial ecosystem functioning. Evergreen broadleaf forests (EBFs) keep leaves throughout the year, and therefore could experience higher drought risks than other biomes. However, the recent temporal variability of global vegetation productivity or land carbon sink is mainly driven by non-evergreen ecosystems, such as semiarid grasslands, croplands, and boreal forests. Thus, we hypothesize that EBFs have higher stability than other biomes under the increasingly extreme droughts. Here we use long-term Standardized Precipitation and Evaporation Index (SPEI) data and satellite-derived Enhanced Vegetation Index (EVI) products to quantify the temporal stability (ratio of mean annual EVI to its SD), resistance (ability to maintain its original levels during droughts), and resilience (rate of EVI recovering to pre-drought levels) at biome and global scales. We identified significantly increasing trends of annual drought severity (SPEI range: −0.08 to −1.80), area (areal fraction range: 2%–19%), and duration (month range: 7.9–9.1) in the EBF biome over 2000–2014. However, EBFs showed the highest resistance of EVI to droughts, but no significant differences in resilience of EVI to droughts were found among biomes (forests, grasslands, savannas, and shrublands). Global resistance and resilience of EVI to droughts were largely affected by temperature and solar radiation. These findings suggest that EBFs have higher stability than other biomes despite the greater drought exposure. Thus, the conservation of EBFs is critical for stabilizing global vegetation productivity and land carbon sink under more-intense climate extremes in the future.

KEYWORDS
droughts, ecosystem stability, Enhanced Vegetation Index, evergreen broadleaf forests, resilience, resistance

1 | INTRODUCTION

Increasingly frequent and severe climate extremes such as droughts and heat waves are expected in the context of future climate warming (Dai, 2013; Easterling et al., 2000; IPCC, 2014; Reichstein et al., 2013; Sippel et al., 2018). Droughts could significantly affect the temporal stability of terrestrial ecosystem functioning, such as photosynthetic capacity (Zhou et al., 2014), ecosystem productivity (Ciais et al., 2005), and land carbon sink (Humphrey et al., 2018;

Jung et al., 2017; Phillips et al., 2009). Further understanding of the effect of droughts on ecosystem functioning benefits the projections of terrestrial feedback to future climate change by Earth system models (Friedlingstein et al., 2006, 2014; Reichstein et al., 2013; Sitch et al., 2008).

Recent studies have identified that the temporal variability of global vegetation productivity or land carbon sink is mainly contributed by non-evergreen ecosystems (Mitchard, 2018), such as semi-arid grasslands (Ahlström et al., 2015; Poulter et al., 2014), cropland

intensification (Gray et al., 2014; Huang et al., 2018; Zeng et al., 2014), and boreal forests (Forkel et al., 2016; Graven et al., 2013; Li, Wu, Liu, Zhang, & Li, 2018; Li, Xia, et al., 2018). Meanwhile, the evergreen broadleaf forests (EBFs; mainly tropical and subtropical evergreen forests) have experienced a trend toward drier (Boisier, Ciais, Ducharne, & Guimberteau, 2015; Malhi et al., 2009) and longer (Fu et al., 2013) dry seasons over the recent decades. The EBFs keep leaves all the year round, and even do not shed leaves under severe water deficit (Xu, Medvigy, Powers, Becknell, & Guan, 2016). The EBFs might have greater exposure to droughts. For example, the averaged drought duration of the Amazon evergreen forests increased from 6.5 months in 2005 to 9 months in 2010 (Anderson et al., 2018; Lewis, Brando, Phillips, Heijden, & Nepstad, 2011). Compared with the 2005 drought, the drought area of Amazonian evergreen forests increased by around 8% during the 2010 drought (Anderson et al., 2018). China's tropical and subtropical EBFs have also suffered from drier soil and more frequent droughts over the recent decades (Wang, Wang, Liu, Zhou, & Yan, 2016; Zhou et al., 2011). We therefore hypothesize that EBFs have high temporal stability of vegetation productivity, defined as the ratio of the temporal mean to its standard deviation (SD), to resist the increasing stress imposed by droughts.

The effect of droughts on ecosystem temporal stability could be generally described by resistance and resilience globally (De Keersmaecker et al., 2015; Tilman & Downing, 1994), and these stability components consider concurrent and delayed effects of droughts on ecosystem (Ivits, Horion, Erhard, & Fensholt, 2016; Pennekamp et al., 2018). Resistance quantifies the direct (concurrent) effect of droughts on ecosystem functioning, expressed as the capacity to maintain its original levels during droughts (Van Ruijven & Berendse, 2010). Resilience defines the rate of ecosystem functioning recovering to its normal state after droughts (De Keersmaecker et al., 2015; Ivits et al., 2016). Experimental and modeling studies have analyzed those two stability components from species to biome level (Anderegg et al., 2015; De Keersmaecker et al., 2015; Gazol et al., 2018; Hoover, Knapp, & Smith, 2014; Hu et al., 2018; Isbell et al., 2015; Ivits et al., 2016; Li, Wu, et al., 2018; Li, Xia, et al., 2018; Schwalm et al., 2017; Van Ruijven & Berendse, 2010). However, direct quantifications of global ecosystem resistance and resilience to droughts by measuring the variations of ecosystem functioning during and after droughts are rare. Thus, how the temporal stability of EBFs, including resistance and resilience, will be affected by droughts remains unclear.

The data availability of satellite-derived vegetation indices for measuring vegetation dynamics has been rapidly increasing in the past decades. The Moderate-resolution Imaging Spectroradiometer (MODIS) Enhanced Vegetation Index (EVI) data, as a proxy of vegetation greenness and productivity, offer opportunities to characterize vegetation photosynthetic dynamics even in areas with high biomass and high coverage area (Huete et al., 2002). Here we identify the global-scale drought occurrences based on the long-term (1901–2014) data of the Standardized Precipitation and Evaporation Index (SPEI), and analyze the yearly trends in drought severity, area,

and duration among biomes over 2000–2014. Using the annual EVI data during 2000–2014, we measure the temporal stability (mean annual EVI/SD), resistance, and resilience of EVI to droughts among biomes and across the globe. Some recent experimental studies have suggested that ecosystem stability is regulated by climate change as well as species richness on the basis of site-level measurements (García-Palacios, Gross, Gaitán, & Maestre, 2018; Shi et al., 2016), so we adopt a machine-learning algorithm to evaluate the relative importance of climatic variables and species richness as the drivers of global resistance and resilience of EVI to droughts. In this study, we formulate and test these hypotheses: (a) EBFs have greater exposure to droughts than other biomes; (b) EBFs have high temporal stability of EVI; and (c) both climate change and species richness influence resistance and resilience of EVI to droughts at the global scale.

2 | MATERIALS AND METHODS

2.1 | Study area and biomes

The MODIS land cover data (MCD12C1, 2011) in this study were obtained from https://lpdaac.usgs.gov/get_data. Our ecosystem stability study was conducted over the vegetated area, excluding the barren land and permanent ice. We also excluded pixels dominated by croplands, because their ecosystem stability under droughts was greatly affected by human management. In this study, the non-crop biomes (Figure S1) include EBF, evergreen needleleaf forest (ENF), deciduous broadleaf forest (DBF), deciduous needleleaf forest (DNF), mixed forest (MF), woody savannas and savannas (SAV), open and closed shrublands (SHR), and grassland (GRA) based on the MODIS land cover product (MCD12C1, 2011).

2.2 | EVI data

The MODIS EVI data were developed to optimize the possible saturation of vegetation signal with improved sensitivity in high-biomass regions (Huete et al., 2002), and it has been widely used as a proxy of canopy "greenness" to address spatial and temporal variations in terrestrial vegetation photosynthetic activity (Ma, Huete, Moran, Ponce-Campos, & Eamus, 2015; Zhou et al., 2014). The monthly MODIS EVI products (MOD13C2; Collection 6) at 0.05° spatial resolution were obtained from the online Data Pool at the NASA Land Processes Distributed Active Archive Centre, U.S. Geological Survey/Earth Resources Observation and Science Centre (http://lpdaac.usgs.gov). The gridded EVI datasets include pixel-level quality assurance (QA) flags as well as statistics of EVI quality and input data. To get high-quality EVI composites, we filtered the original data using the following the previous criteria (Ma et al., 2015) based on the QA layers: (a) corrected product produced at ideal quality for all bands; (b) highest quality for bands 1–7; (c) atmospheric correction; (d) adjacency correction; (e) MOD35 cloud flag indicated "clear"; (f) no detections of cloud-shadow; and (g) low or average aerosol quantities. Gaps remaining after QA filtering were filled by interpolation in the temporal dimension,

computing the values of gaps by fitting linearly between the two adjacent points. The time series with more than two consecutive gaps were excluded from further analyses. The data were then mosaicked and re-projected by using the MODIS Reprojection Tool, and mosaicked images resampled into 0.5° × 0.5° (latitude × longitude) resolution by using the nearest neighbor algorithm to match the resolution of global drought indices data and global climate forcing datasets. The equation defining EVI is:

$$EVI = 2.5 \times \frac{\rho_{nir} - \rho_{red}}{\rho_{nir} + 6 \times \rho_{red} - 7.5 \times \rho_{blue} + 1}, \tag{1}$$

where ρ_{nir}, ρ_{red}, and ρ_{blue} are reflectance of the near infrared (841–876 nm), red (620–670 nm), and blue (459–479 nm) bands of the MODIS sensor, respectively.

In this study, all the MOD13C2 EVI data at monthly resolution were aggregated to annual mean for each grid, and we characterized drought-induced vegetation greenness changes with annual EVI during 2000–2014.

2.3 | Identifying drought and wetness events

To identify and quantify annual climate events, we used the SPEI (version 2.4) over the past century (1901–2014) on 0.5° × 0.5° grids to define each year as "extreme" (dryness or wetness) or "normal" condition at the pixel level (Vicente-Serrano, Beguería, & López-Moreno, 2009). SPEI (http://sac.csic.es/spei/database.html) is a global and gridded drought metric with respect to the long-term water balance, calculated as the difference between monthly precipitation and potential evapotranspiration from the Climatic Research Unit (CRU) TS 4.01 dataset (http://www.cru.uea.ac.uk/cru/data/hrg/). This multiscalar metric represents either a water surplus or deficit for a given month and are then aggregated over the integration timescale from 3 to 24 months (Schwalm et al., 2017; Vicente-Serrano et al., 2013). After these aggregation schemes, the value normalized by a three-parameter log-logistic distribution is the SPEI index (Schwalm et al., 2017). For example, a 12 month SPEI value for a given month represents the cumulative water balance over the preceding 12 months. The SPEI metric was relative to the conditions at the site for which it was calculated, with a value of 0 representing averaged drought conditions, positive values denoting higher than averaged water availability, and negative values denoting drier conditions. Here we used SPEI that was integrated at the 12 month time scale (hereafter SPEI-12) to monitor the effect of annual water balance on vegetation productivity. Longer timescales SPEI was more sensible to identify hydrological droughts compared with shorter timescales targeting meteorological and/or agricultural droughts (Ivits, Horion, Fensholt, & Cherlet, 2013), and plant germination in several biomes was mainly controlled by the precipitation accumulated over the previous 12 months (Vicente-Serrano, 2006).

To calculate the grid-specific thresholds for annual extreme drought and wetness, the gridded SPEI-12 products at a monthly resolution were aggregated to an annual mean. Based on the SPEI-12 data aggregated at annual resolution, we defined the thresholds for annual extreme events (extreme drought or extreme wetness years) as those dry events (negative SPEI values) or wet events (positive SPEI values) occurring less frequently than once per decade (10% of observations) over the past century (1901–2014) at each grid cell. The grid-specific SPEI-12 thresholds were used to screen for extreme drought and wetness events, and therefore 20% of the SPEI historic climate years (114 years) were identified as extreme drought events plus extreme wetness events. Normal years were defined as those within the range between the drought threshold and wetness threshold. Note that here we only recorded the extreme events and normal years occurred over the past 15 years (2000–2014), corresponding to the EVI satellite monitoring.

The annual drought period starts from the first month when the SPEI-12 is lower than a drought threshold, lasting at least three consecutive months, and ends to the last month before the SPEI-12 is larger than the drought threshold (Schwalm et al., 2017). All the drought periods identified in the same year were then summed up to the annual drought duration. Note that here we only recorded the extreme events and normal years occurred over the past 15 years (2000–2014), corresponding to the EVI satellite monitoring.

2.4 | Stability components

The temporal stability (S) of EVI is defined as μ/δ, where μ is the mean annual EVI across all the years and δ is its temporal SD of the same time interval (Tilman, Reich, & Knops, 2006). In order to disentangle the effect of annual EVI trend on temporal stability calculation, we also calculated detrended temporal stability (S_d) for each grid cell. The detrended temporal stability was $S_d = \mu/\delta_d$. Detrending was done by linear regression of annual EVI and year at the grid cell, and δ_d is the SD of residuals for each regression (Tilman et al., 2006).

Two components of temporal stability, including resistance and resilience, were used to evaluate the effect of climate extremes on temporal stability of EVI. Here resistance describes the ability of EVI to maintain its original levels during the droughts, while resilience measures the rate of EVI recovering to its pre-drought level (De Keersmaecker et al., 2014; Van Ruijven & Berendse, 2010). Similar to the description in Isbell et al. (2015), resistance (Ω) and resilience (Δ) were calculated as follows:

$$\Omega = \frac{\overline{Y_n}}{|Y_e - \overline{Y_n}|} \tag{2}$$

$$\Delta = \left| \frac{Y_e - \overline{Y_n}}{Y_{e+1} - \overline{Y_n}} \right| \tag{3}$$

where $\overline{Y_n}$, Y_e, and Y_{e+1} represent the expected EVI during normal years (mean across all the non-extreme years), during the year climate extremes occurred, and during the year after a climate extreme, respectively. The results derived from Schwalm et al. (2017) show that >95% of the global vegetated area can recover from droughts in 1 year (Figure S2), and the biome-level drought recovery time is within 1 year

(Schwalm et al., 2017). Therefore, the above resilience index was used to analyze the biome-scale resilience in this study.

The indices of resistance and resilience used in this study are unitless, and thus could be directly comparable among biomes with different productivity levels. Those two indices are also symmetric, and thus could be comparable between wet events and dry events. Greater resistance suggests less vegetation EVI reduced during the droughts. If the drought event lowers the vegetation greenness, higher increasing rates of EVI during the recovery lead to greater resilience. In addition, if the rapid recovery rate overshoots its normal level, it will lead to progressively lower resilience (Isbell et al., 2015). For example, if vegetation EVI is reduced during a drought to half its normal levels (Y_n), then $\Omega = 2$. If 1 year after a drought vegetation EVI recovers either from 50% to 75% or from 50% to 125% of its normal levels, then the vegetation EVI will return halfway from disturbed to normal levels, and $\Delta = 2$. A higher value of Ω or Δ represents a higher resistance or resilience, and a lower value of Ω or Δ represents instability.

2.5 | Climate forcing and species richness datasets

Climate forcing and species richness datasets were used to investigate the relative contributions of multiple drivers to global resistance and resilience of EVI to droughts. The annual gridded air temperature and precipitation data were obtained from CRU TS 4.02 with a spatial resolution of 0.5° × 0.5° (Harris, Jones, Osborn, & Lister, 2014). We obtained 0.5° × 0.5° gridded data of annual downward shortwave solar radiation at the surface (W/m^2) from the Terrestrial Hydrology Research Group at Princeton University (Sheffield, Goteti, & Wood, 2006). The gridded normalized species richness data of native species (Ellis, Antill, & Kreft, 2012) were used as a metric to quantify plant biodiversity globally. Here we used species richness and the annual means of climate factors (including air temperature, precipitation, and shortwave solar radiation) to analyze the contributions to resistance and resilience of EVI.

2.6 | Statistical analysis

The temporal trends in annual drought metrics, including severity, area, and duration, for each biome were estimated by the Theil–Sen slope estimator (referred to here as Sen's slope; Sen, 1968). To test whether the EBFs have higher stability and its two components than other biomes, we used a one-way analysis of variance to evaluate the differences in the mean values among different biomes (using biome as the main factor). $p < .05$ was considered as statistically significant.

We conducted a random forest regression analysis (Bertrand et al., 2011) to identify the most important predictors of spatial variation in resistance and resilience. The predictors include mean annual temperature (MAT), mean annual precipitation (MAP), mean annual shortwave radiation (MAR), and species richness. The random forest analysis could account for interactions and nonlinear relationships between predictors (Gill et al., 2017), and could deal with the multicollinearity problems in multivariate regression (Delgado-Baquerizo

et al., 2017). The fit for each tree is determined by randomly selecting cases. The importance of each predictor variable is determined by the percentage increase in the mean square error (%IncMSE) between observations and predictions, and the decrease is averaged over all the trees to produce the final estimation for importance (Delgado-Baquerizo et al., 2017). Greater values of %IncMSE denote higher variable importance. In this study, the importance measure was calculated for each tree and averaged over the forest (1,000 trees). These variable importance analyses were conducted using the randomForest package in R.

All analyses were conducted using R (http://www.r-project.org/).

3 | RESULTS

3.1 | Drought exposure among different biomes

Among the eight biomes, only EBF exhibited significantly increasing trends in annual drought severity ($p < .001$, Figure 1a), area ($p < .001$, Figure 1b), and duration ($p < .001$, Figure 1c) over the period 2000–2014, and DNF showed an increasing trend in annual drought severity ($p < .05$, Figure 1a). EBF contained a large proportion of global aboveground biomass carbon (Figure 1a inset). The spatially-averaged SPEI values of drought regions decreased from −0.08 to −1.80 ($r^2 = .8$; $p < .001$) during the period 2000–2014, suggesting significantly enhanced drought severity through time in EBF (Figure 1a). The DNF also experienced an increasing trend of drought severity over the past decades ($r^2 = .41$; $p < .05$). No significant trend of drought severity was observed in the remaining biomes. Additionally, EBF contained nearly half (47.7%) of the global aboveground biomass carbon, while DNF only accounted for 1.7% of the global aboveground biomass carbon (Figure 1a inset). Meanwhile, we identified the spatial pattern of drought occurrences during the period 2000–2014 (Figure S3). Our analysis showed a significantly increasing trend of drought area in EBF over 2000–2014 ($p < .001$), and no significant trend of drought area through time was identified in the remaining biomes (Figure 1b). Averaged drought duration for EBF significantly increased from 7.9 to 9.1 months ($p < .001$, Figure 1c).

3.2 | Stability components of EVI to droughts among different biomes

The temporal stability (the inverse of the coefficient of variation) of EVI exhibited large spatial variability at the global scale (Figure 2a). High temporal stability of EVI was identified in tropical regions, whereas low temporal stability of EVI were identified in arid biomes and high northern latitudes (Figure 2a; Figure S1). The EBF illustrated significantly higher temporal stability of EVI to droughts ($p < .001$, Figure 3a; Table S1) than other biomes.

The resistance of EVI to droughts also exhibited contrasting spatial variability at the global scale (Figure 2b), and the EBF illustrated significantly higher resistance of EVI ($p < .001$, Figure 3b; Table S1) than other biomes. The EBF also showed higher detrended temporal stability of EVI than other biomes (Figure S4).
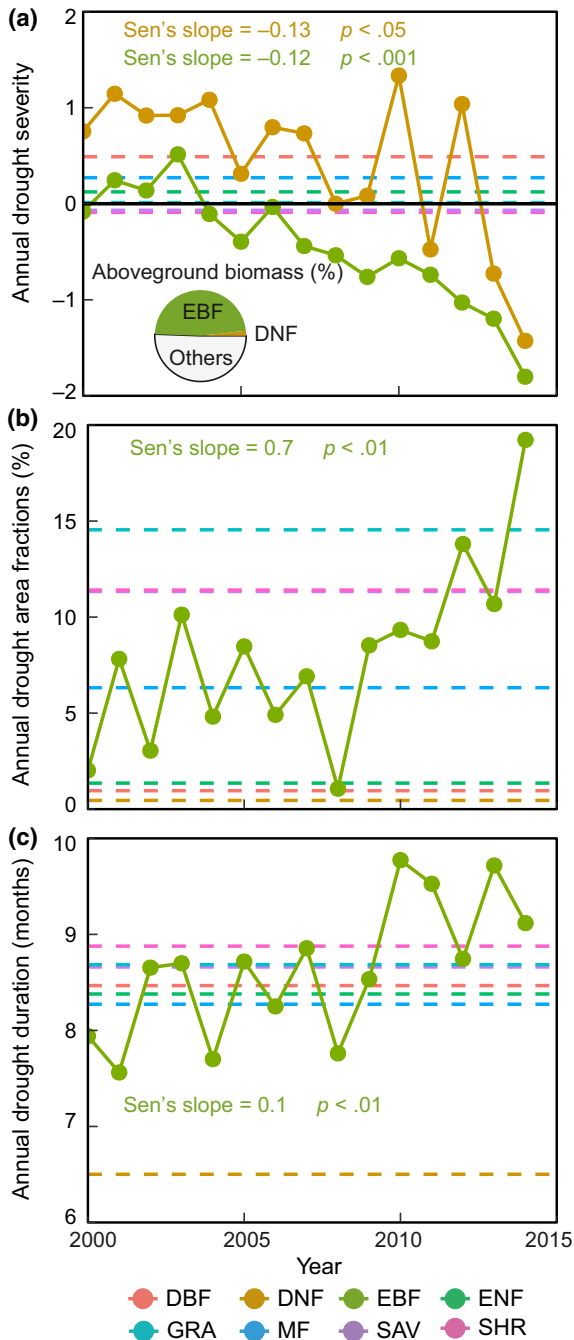
FIGURE 1 Temporal dynamics of annual drought severity (a), area (b), and duration (c) across the non-crop biomes during 2000–2014. (a) Averaged pixel-level SPEI-12 values of the drought regions. More negative ones indicate more severe droughts relative to normal conditions. (b) The areal fractions of identified drought over lands at the biome level. (c) Drought duration (month) over lands at the biome level. All values are spatially averaged within the biome. As there were no significant relationships ($p > .05$) with time, the multi-year mean for each biome is shown as a dashed line. Inset pie chart shows the percentages (%) of vegetation optical depth-based aboveground biomass (Liu et al., 2015) for each biome in 2000. Non-crop biome types: DBF (deciduous broadleaf forest), DNF (deciduous needleleaf forest), EBF (evergreen broadleaf forest), ENF (evergreen needleleaf forest), GRA (grassland), MF (mixed forest), SAV (savannah), and SHR (shrubland)

For the resilience of EVI to droughts, similar recovering rates (mean ± SD; 2.63 ± 1.29) of EVI were identified across different regions (Figure 2c), and no significant difference in resilience of EVI to drought was detected between EBF and the other biomes (Figure 3c; Table S1).

3.3 | Relative contribution of climate change and species richness to resistance and resilience

Among the climatic factors and species richness, MAR and MAT were the main drivers of resistance and resilience of EVI at the global scale (Figure 4). The most important predictor of global resistance of EVI to droughts was MAR (%IncMSE = 14.9%), followed by MAT (%IncMSE = 12.8%). Species richness (%IncMSE = 11%) and MAP (%IncMSE = 7.7%) were of secondary importance to the resistance of EVI (Figure 4a). MAR, MAT, species richness, and MAP were positively associated with the global resistance of EVI to droughts ($p < .05$, Table S2). As illustrated in Figure 4b, the most important predictors of resilience to droughts were MAT (%IncMSE = 12.8%) and MAR (%IncMSE = 11.9%). Other predictors of secondary importance to resilience of EVI were MAP (%IncMSE = 10.8%) and species richness (%IncMSE = 10.5%).

4 | DISCUSSION

This study detects a higher drought resistance of vegetation productivity in EBFs than in other biomes, which could be driven by different mechanisms. First, increasing light exposure during the onset of droughts in the wet-to-dry season of the tropical evergreen forests might lead to consistent and even enhanced canopy greenness. Radiation, rather than water availability, is regarded as the main limiting factor for tropical evergreen forests (Guan et al., 2015; Nemani et al., 2003; Saleska et al., 2016; Seddon, Macias-Fauria, Long, Benz, & Willis, 2016; Tang & Dubayah, 2017). Evidence from ground observations (Saleska et al., 2016; Wu et al., 2016) and satellites (Liu et al., 2018; Tang & Dubayah, 2017) has shown that new leaf development and therefore increasing leaf area index is largely driven by higher radiation during the annual dry season. Second, the increasing canopy light use efficiency (LUE) of tropical evergreen forests during the annual dry season may enhance the resistance of plant photosynthesis to droughts in EBFs. Tropical evergreen forest canopies tend to maintain more light use-efficient leaves by flushing newly leaves of high photosynthetic capacity and dropping old leaves before droughts during the dry season (Tang & Dubayah, 2017; Wu et al., 2016, 2017). The canopy LUE in the dry season is not limited by water stress (Guan et al., 2015; Wu et al., 2017), and evidence from FLUXNET towers (Wei, Yi, Fang, & Hendrey, 2017) and a field survey (Wu et al., 2016) in tropical evergreen forests also has shown an increasing trend in LUE over the annual dry season. Third, the seasonal maximum air temperature in most EBFs is still lower than the optimal temperature of canopy photosynthetic capacity (Huang et al., 2019). Despite the high temperature

FIGURE 2 Global pattern of temporal stability (a) of Enhanced Vegetation Index (EVI), resistance (b), and resilience (c) of EVI to droughts. (a) Temporal stability (ratio of mean annual EVI to its *SD*), resistance (b), and resilience (c) of EVI to droughts in each grid cell are calculated from annual EVI using the algorithm in Section 2.2. Black dots in (a) indicate the vegetated areas with droughts identified. White areas in (b) and (c) indicate those areas with non-vegetation and non-occurrences of droughts detected here
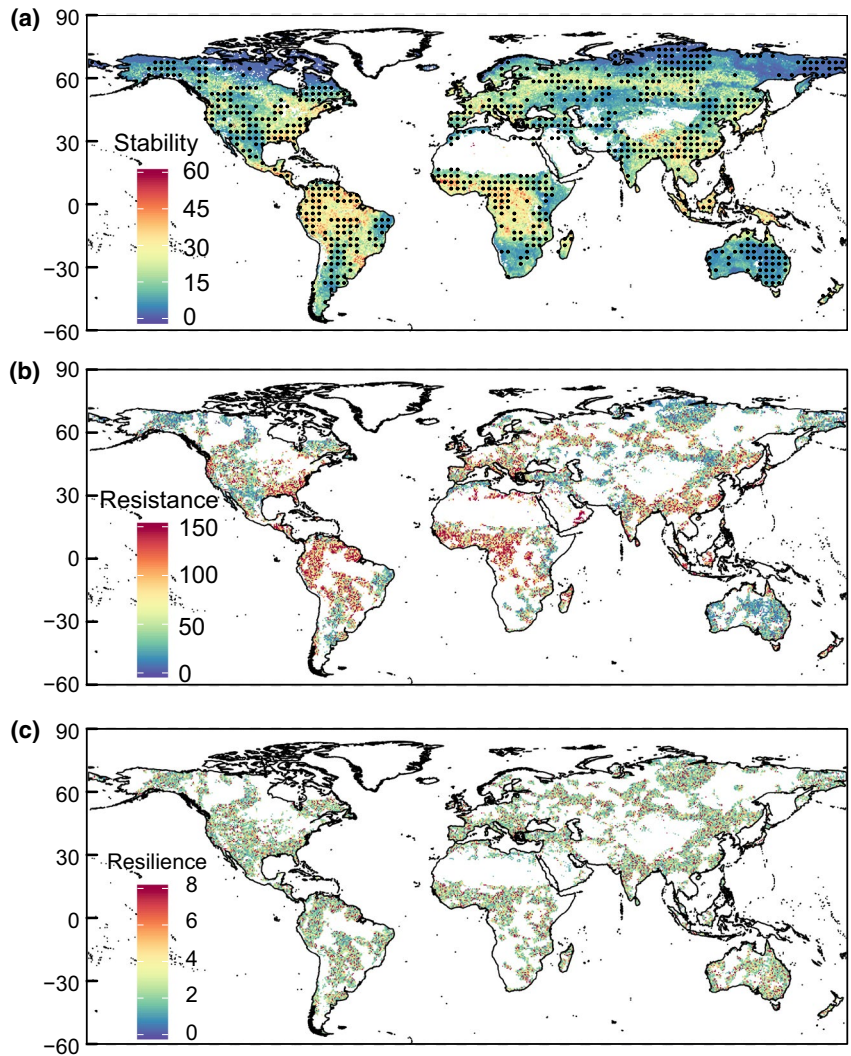

FIGURE 3 Comparisons of temporal stability (a), resistance (b), and resilience (c) of EVI to droughts among different biomes. The values of points and error bars in (a) indicate means ± 10*SEM* for each biome. The lines across the box in (b) and (c) indicate the mean values, and lower and upper boxes show the interquartile range (25th and 75th percentiles). Whiskers (the lines on the ending of boxes) correspond to 1.5 times the inter-quartile range. DBF, deciduous broadleaf forest; DNF, deciduous needleleaf forest; EBF, evergreen broadleaf forest; ENF, evergreen needleleaf forest; GRA, grassland; MF, mixed forest; SAV, savannah; SHR, shrubland
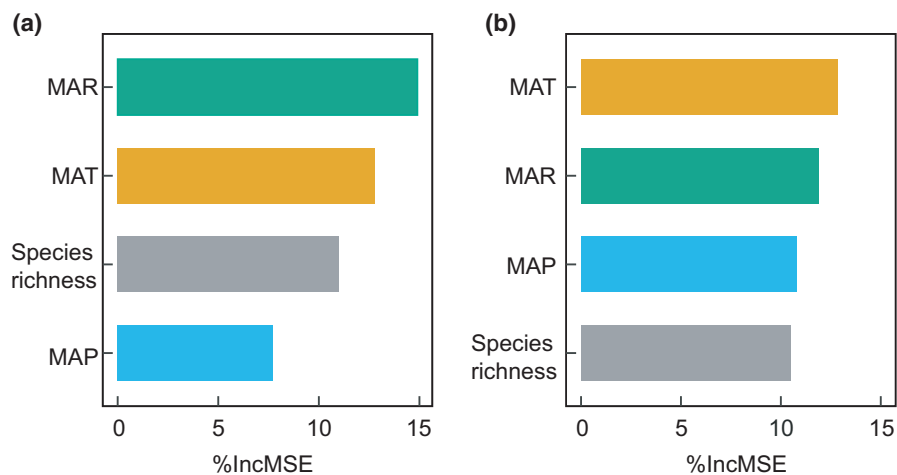
(a)

(b)
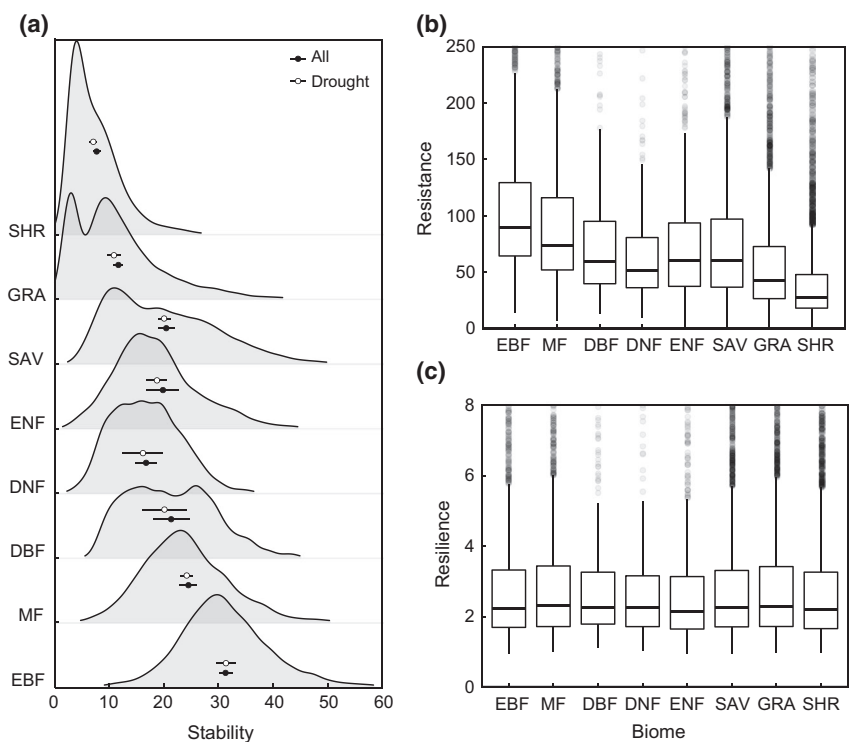
FIGURE 4 Relative contributions of the predictor variables in the random forest model denoted by percentage increase of mean squared error. Values of the percentage increase of mean squared error (%IncMSE) are generated from 1,000 trees of the global ecosystem resistance (a) and ecosystem resilience (b). MAR, MAT, and MAP represent mean annual shortwave radiation, mean annual temperature, and mean annual precipitation, respectively. The species richness data are available from http://ecotope.org/anthromes/biodiversity/plants/data/

during droughts, the safe operating space between air temperature and thermal optimum of photosynthesis would provide EBFs with a thermal buffer against the impacts of warming on ecosystem photosynthesis in the dry season (Way, 2019; Wu et al., 2017). In fact, some studies have revealed a high sensitivity of vegetation productivity to the combination of light and temperature variability in tropical regions (Nemani et al., 2003; Seddon et al., 2016). Our analysis of relative contributions also indicates that solar radiation and temperature are predicted to be more important than species richness in driving resistance and resilience of EVI to droughts at the global scale (Figure 4). All these physiological aspects could collectively make the EBFs more stable and resistant to droughts than the rest of the biomes.

The similar resilience of EVI to droughts among biomes (Figure 3c) is largely due to the common range of cross-biome water use efficiency (WUE) under altered water availability. A previous study has documented that large-scale ecological resilience could be indicated by ecosystem-level WUE, which is convergent across contrasting hydroclimatic conditions (Ponce-Campos et al., 2013). In other words, WUE is conservative among biomes ranging from grassland to forest, irrespective of hydroclimatic conditions. This intrinsic sensitivity of vegetation to water availability across precipitation gradients supports our findings that there are no significant differences in the resilience of EVI to droughts. In addition, our results are consistent with the quantitative analysis of global-scale vegetation sensitivity to three climatic variables by Seddon et al. (2016), both of which find similar vegetation sensitivity to climate variability among biomes (Figure S5).

The high stability of EBFs observed in this study suggests a key role of EBFs in stabilizing global vegetation productivity despite severe droughts, and could be reconciled with the contributions of non-evergreen ecosystems to temporal variability of the land carbon sink (Ahlström et al., 2015; Forkel et al., 2016; Graven et al., 2013; Gray et al., 2014; Huang et al., 2018; Poulter et al., 2014; Zeng et al., 2014). Terrestrial vegetation productivity or photosynthetic carbon uptake is the main driver of the land carbon sink (Anav et al., 2015) and the foundation of global carbon cycle (Running, 2012). Temporal variability of vegetation productivity is largely associated with extreme droughts over the past three decades (Reichstein et al., 2013; Jakob

et al., 2014), and EBFs account for about 60% of the global photosynthetic carbon uptake (Mitchard, 2018). Given the increasingly severe droughts in the future (Dai, 2013; Reichstein et al., 2013; Sippel et al., 2018), whether the stability of EBFs will reduce remains unclear. What's more, some recent evidence has shown that deforestation of EBFs (e.g., conversion to croplands) has widely occurred in the recent past (Duveiller, Hooker, & Cescatti, 2018). Our work highlights the urgent need of the conservation of EBFs on the global scale.

The global analysis of ecosystem resistance and resilience derived from remote-sensed vegetation index is an attempt to diagnose the ecosystem-scale stability of vegetation productivity and its possible ecophysiological mechanisms under increasing droughts. However, it should be noted that our study does not fully account for the complex site-level responses to long-term droughts, such as drought-induced tree mortality (Allen et al., 2010; Doughty et al., 2015; Phillips et al., 2009) and post-drought fires (Saatchi et al., 2013). Tropical evergreen forests often display positive and negative responses to droughts (McDowell et al., 2018). For example, Amazonian droughts benefit vegetation growth in part via increasing photosynthetic capacity (Saleska et al., 2016; Wagner et al., 2017), flushing of young leaves (Wu et al., 2016), and above-average solar radiation (Guan et al., 2015). Nonetheless, droughts sometimes lead to increasing tree mortality and reduced biomass (Doughty et al., 2015; Phillips et al., 2009). With cautious interpretation of the high ecosystem stability of EBFs under severe droughts, ground observations and continuous satellite records are needed in future research to fully understand the post-drought dynamics of both canopy and understory vegetation.

In summary, the results of this study suggest that EBFs have experienced greater exposure to droughts, but have a higher stability than other biomes. We found that the high stability of EBFs primarily resulted from their higher resistance to droughts. Our findings imply that EBFs are critical in stabilizing the global vegetation productivity and land carbon sink under future droughts. Given that the current generation of global vegetation models have a large uncertainty in EBFs (e.g., Cui et al., 2019) and usually underestimate the impacts of climate extremes such as droughts

(Schewe et al., 2019), this study underscores the importance of process-level understanding of vegetation stability in response to extreme droughts.

ORCID

Kun Huang https://orcid.org/0000-0002-7469-6085

Jianyang Xia https://orcid.org/0000-0001-5923-6665

REFERENCES

Ahlstrom, A., Raupach, M. R., Schurgers, G., Smith, B., Arneth, A., Jung, M., ... Zeng, N. (2015). The dominant role of semi-arid ecosystems in the trend and variability of the land CO_2 sink. *Science*, *348*, 895–899. https://doi.org/10.1126/science.aaa1668

Allen, C. D., Macalady, A. K., Chenchouni, H., Bachelet, D., McDowell, N., Vennetier, M., ... Cobb, N. (2010). A global overview of drought and heat-induced tree mortality reveals emerging climate change risks for forests. *Forest Ecology and Management*, *259*, 660–684. https://doi.org/10.1016/j.foreco.2009.09.001

Anav, A., Friedlingstein, P., Beer, C., Ciais, P., Harper, A., Jones, C., & Zhao, M. (2015). Spatiotemporal patterns of terrestrial gross primary production: A review. *Reviews of Geophysics*, *53*, 785–818. https://doi.org/10.1002/2015RG000483

Anderegg, W. R. L., Schwalm, C., Biondi, F., Camarero, J. J., Koch, G., Litvak, M., ... Pacala, S. (2015). Pervasive drought legacies in forest ecosystems and their implications for carbon cycle models. *Science*, *349*, 528–532. https://doi.org/10.1126/science.aab1833

Anderson, L. O., Ribeiro Neto, G., Cunha, A. P., Fonseca, M. G., Mendes de Moura, Y., Dalagnol, R., ... de Aragão, L. E. O. E. C. (2018). Vulnerability of Amazonian forests to repeated droughts. *Philosophical Transactions of the Royal Society B: Biological Sciences*, *373*, 20170411. https://doi.org/10.1098/rstb.2017.0411

Bertrand, R., Lenoir, J., Piedallu, C., Riofrío-Dillon, G., de Ruffray, P., Vidal, C., ... Gégout, J.-C. (2011). Changes in plant community composition lag behind climate warming in lowland forests. *Nature*, *479*, 517–520. https://doi.org/10.1038/nature10548

Boisier, J. P., Ciais, P., Ducharne, A., & Guimberteau, M. (2015). Projected strengthening of Amazonian dry season by constrained climate model simulations. *Nature Climate Change*, *5*, 656–661. https://doi.org/10.1038/nclimate2658

Ciais, P. H., Reichstein, M., Viovy, N., Granier, A., Ogée, J., Allard, V., ... Valentini, R. (2005). Europe-wide reduction in primary productivity caused by the heat and drought in 2003. *Nature*, *437*, 529–533. https://doi.org/10.1038/nature03972

Cui, E., Huang, K., Arain, M. A., Fisher, J. B., Huntzinger, D. N., Ito, A., ... Xia, J. (2019). Vegetation functional properties determine uncertainty of simulated ecosystem productivity: A traceability analysis in the East Asian monsoon region. *Global Biogeochemical Cycles*, *33*, 2018GB005909. https://doi.org/10.1029/2018GB005909

Dai, A. (2013). Increasing drought under global warming in observations and models. *Nature Climate Change*, *3*, 52–58. https://doi.org/10.1038/NCLIMATE1633

De Keersmaecker, W., Lhermitte, S., Honnay, O., Farifteh, J., Somers, B., & Coppin, P. (2014). How to measure ecosystem stability? An evaluation of the reliability of stability metrics based on remote sensing time series across the major global ecosystems. *Global Change Biology*, *20*, 2149–2161. https://doi.org/10.1111/gcb.12495

De Keersmaecker, W., Lhermitte, S., Tits, L., Honnay, O., Somers, B., & Coppin, P. (2015). A model quantifying global vegetation resistance and resilience to short-term climate anomalies and their relationship with vegetation cover. *Global Ecology and Biogeography*, *24*, 539–548. https://doi.org/10.1111/geb.12279

Delgado-Baquerizo, M., Eldridge, D. J., Maestre, F. T., Karunaratne, S. B., Trivedi, P., Reich, P. B., & Singh, B. K. (2017). Climate legacies drive global soil carbon stocks in terrestrial ecosystems. *Science Advances*, *3*, e1602008. https://doi.org/10.1126/sciadv.1602008

Doughty, C. E., Metcalfe, D. B., Girardin, C. A. J., Amézquita, F. F., Cabrera, D. G., Huasco, W. H., ... Malhi, Y. (2015). Drought impact on forest carbon dynamics and fluxes in Amazonia. *Nature*, *519*, 78–82. https://doi.org/10.1038/nature14213

Duveiller, G., Hooker, J., & Cescatti, A. (2018). The mark of vegetation change on Earth's surface energy balance. *Nature Communications*, *9*, 679. https://doi.org/10.1038/s41467-017-02810-8

Easterling, D. R., Meehl, G. A., Parmesan, C., Changnon, S. A., Karl, T. R., & Mearns, L. O. (2000). Climate extremes: Observations, modeling, and impacts. *Science*, *289*, 2068–2074. https://doi.org/10.1126/science.289.5487.2068

Ellis, E. C., Antill, E. C., & Kreft, H. (2012). All is not loss: Plant biodiversity in the Anthropocene. *PLoS ONE*, *7*, e30535. https://doi.org/10.1371/journal.pone.0030535

Forkel, M., Carvalhais, N., Rodenbeck, C., Keeling, R., Heimann, M., Thonicke, K., ... Reichstein, M. (2016). Enhanced seasonal CO_2 exchange caused by amplified plant productivity in northern ecosystems. *Science*, *351*, 696–699. https://doi.org/10.1126/science.aac4971

Friedlingstein, P., Cox, P. M., Betts, R., Bopp, L., von Bloh, W., Brovkin, V., ... Zeng, N. (2006). Climate-carbon cycle feedback analysis: Results from the C4MIP model intercomparison. *Journal of Climate*, *19*, 3337–3353. https://doi.org/10.1175/jcli3800.1

Friedlingstein, P., Meinshausen, M., Arora, V. K., Jones, C. D., Anav, A., Liddicoat, S. K., & Knutti, R. (2014). Uncertainties in CMIP5 climate projections due to carbon cycle feedbacks. *Journal of Climate*, *27*, 511–526. https://doi.org/10.1175/jcli-d-12-00579.1

Fu, R., Yin, L., Li, W., Arias, P. A., Dickinson, R. E., Huang, L., ... Myneni, R. B. (2013). Increased dry-season length over southern Amazonia in recent decades and its implication for future climate projection. *Proceedings of the National Academy of Sciences of the United States of America*, *110*, 18110–18115. https://doi.org/10.1073/pnas.1302584110

García-Palacios, P., Gross, N., Gaitán, J., & Maestre, F. T. (2018). Climate mediates the biodiversity–ecosystem stability relationship globally. *Proceedings of the National Academy of Sciences of the United States of America*, *115*, 8400–8405. https://doi.org/10.1073/pnas.1800425115

Gazol, A., Camarero, J. J., Vicente-Serrano, S. M., Sánchez-Salguero, R., Gutiérrez, E., de Luis, M., ... Galván, J. D. (2018). Forest resilience to drought varies across biomes. *Global Change Biology*, *24*, 2143–2158. https://doi.org/10.1111/gcb.14082

Gill, D. A., Mascia, M. B., Ahmadia, G. N., Glew, L., Lester, S. E., Barnes, M., ... Fox, H. E. (2017). Capacity shortfalls hinder the performance of marine protected areas globally. *Nature*, *543*, 665–669. https://doi.org/10.1038/nature21708

Graven, H. D., Keeling, R. F., Piper, S. C., Patra, P. K., Stephens, B. B., Wofsy, S. C., ... Bent, J. D. (2013). Enhanced seasonal exchange of CO_2 by northern ecosystems since 1960. *Science*, *341*, 1085–1089. https://doi.org/10.1126/science.1239207

Gray, J. M., Frolking, S., Kort, E. A., Ray, D. K., Kucharik, C. J., Ramankutty, N., & Friedl, M. A. (2014). Direct human influence on atmospheric CO_2 seasonality from increased cropland productivity. *Nature*, 515, 398–401. https://doi.org/10.1038/nature13957

Guan, K., Pan, M., Li, H., Wolf, A., Wu, J., Medvigy, D., ... Lyapustin, A. I. (2015). Photosynthetic seasonality of global tropical forests constrained by hydroclimate. *Nature Geoscience*, 8, 284–289. https://doi.org/10.1038/ngeo2382

Harris, I., Jones, P. D., Osborn, T. J., & Lister, D. H. (2014). Updated high-resolution grids of monthly climatic observations – The CRU TS3.10 Dataset. *International Journal of Climatology*, 34, 623–642. https://doi.org/10.1002/joc.3711

Hoover, D. L., Knapp, A. K., & Smith, M. D. (2014). Resistance and resilience of a grassland ecosystem to climate extremes. *Ecology*, 95, 2646–2656. https://doi.org/10.1890/13-2186.1

Hu, Z., Guo, Q., Li, S., Piao, S., Knapp, A. K., Ciais, P., ... Yu, G. (2018). Shifts in the dynamics of productivity signal ecosystem state transitions at the biome-scale. *Ecology Letters*, 21, 1457–1466. https://doi.org/10.1111/ele.13126

Huang, K., Xia, J., Wang, Y., Ahlström, A., Chen, J., Cook, R. B., ... Luo, Y. (2018). Enhanced peak growth of global vegetation and its key mechanisms. *Nature Ecology & Evolution*, 2, 1897–1905. https://doi.org/10.1038/s41559-018-0714-0

Huang, M., Piao, S., Ciais, P., Peñuelas, J., Wang, X., Keenan, T. F., ... Janssens, I. A. (2019). Air temperature optima of vegetation productivity across global biomes. *Nature Ecology & Evolution*, 3, 772–779. https://doi.org/10.1038/s41559-019-0838-x

Huete, A., Didan, K., Miura, T., Rodriguez, E. P., Gao, X., & Ferreira, L. G. (2002). Overview of the radiometric and biophysical performance of the MODIS vegetation indices. *Remote Sensing of Environment*, 83, 195–213. https://doi.org/10.1016/S0034-4257(02)00096-2

Humphrey, V., Zscheischler, J., Ciais, P., Gudmundsson, L., Sitch, S., & Seneviratne, S. I. (2018). Sensitivity of atmospheric CO_2 growth rate to observed changes in terrestrial water storage. *Nature*, 560, 628–631. https://doi.org/10.1038/s41586-018-0424-4

IPCC. (2014). Climate change 2014: Impacts, adaptation, and vulnerability. Part A: Global and sectoral aspects. In C. B. Field, V. R. Barros, D. J. Dokken, M. D. Mastrandrea, K. J. Mach, T. E. Bilir, & L. L. White (Eds.), *Contribution of working group II to the fifth assessment report of the Intergovernmental Panel on Climate Change* (pp. 1–65). Cambridge, UK: Cambridge University Press.

Isbell, F., Craven, D., Connolly, J., Loreau, M., Schmid, B., Beierkuhnlein, C., ... Eisenhauer, N. (2015). Biodiversity increases the resistance of ecosystem productivity to climate extremes. *Nature*, 526, 574–577. https://doi.org/10.1038/nature15374

Ivits, E., Horion, S., Erhard, M., & Fensholt, R. (2016). Assessing European ecosystem stability to drought in the vegetation growing season. *Global Ecology and Biogeography*, 25, 1131–1143. https://doi.org/10.1111/geb.12472

Ivits, E., Horion, S., Fensholt, R., & Cherlet, M. (2013). Drought footprint on European ecosystems between 1999 and 2010 assessed by remotely sensed vegetation phenology and productivity. *Global Change Biology*, 20, 581–593. https://doi.org/10.1111/gcb.12393

Jung, M., Reichstein, M., Schwalm, C. R., Huntingford, C., Sitch, S., Ahlström, A., ... Zeng, N. (2017). Compensatory water effects link yearly global land CO_2 sink changes to temperature. *Nature*, 541, 516–520. https://doi.org/10.1038/nature20780

Lewis, S. L., Brando, P. M., Phillips, O. L., van der Heijden, G. M. F., & Nepstad, D. (2011). The 2010 Amazon drought. *Science*, 331, 554. https://doi.org/10.1126/science.1200807

Li, D., Wu, S., Liu, L., Zhang, Y., & Li, S. (2018). Vulnerability of the global terrestrial ecosystems to climate change. *Global Change Biology*, 24, 4095–4106. https://doi.org/10.1111/gcb.14327

Li, Z., Xia, J., Ahlström, A., Rinke, A., Koven, C., Hayes, D. J., ... Luo, Y. (2018). Non-uniform seasonal warming regulates vegetation greening and

atmospheric CO_2 amplification over northern lands. *Environmental Research Letters*, 13, 124008. https://doi.org/10.1088/1748-9326/aae9ad

Liu, Y. Y., van Dijk, A. I. J. M., de Jeu, R. A. M., Canadell, J. G., McCabe, M. F., Evans, J. P., & Wang, G. (2015). Recent reversal in loss of global terrestrial biomass. *Nature Climate Change*, 5, 470–474. https://doi.org/10.1038/nclimate2581

Liu, Y. Y., van Dijk, A. I. J. M., Miralles, D. G., McCabe, M. F., Evans, J. P., de Jeu, R. A. M., ... Restrepo-Coupe, N. (2018). Enhanced canopy growth precedes senescence in 2005 and 2010 Amazonian droughts. *Remote Sensing of Environment*, 211, 26–37. https://doi.org/10.1016/j.rse.2018.03.035

Ma, X., Huete, A., Moran, S., Ponce-Campos, G., & Eamus, D. (2015). Abrupt shifts in phenology and vegetation productivity under climate extremes. *Journal of Geophysical Research: Biogeosciences*, 120, 2036–2052. https://doi.org/10.1002/2015JG003144

Malhi, Y., Aragao, L. E. O. C., Galbraith, D., Huntingford, C., Fisher, R., Zelazowski, P., ... Meir, P. (2009). Exploring the likelihood and mechanism of a climate-change-induced dieback of the Amazon rainforest. *Proceedings of the National Academy of Sciences of the United States of America*, 106, 20610–20615. https://doi.org/10.1073/pnas.0804619106

McDowell, N., Allen, C. D., Anderson-Teixeira, K., Brando, P., Brienen, R., Chambers, J., ... Xu, X. (2018). Drivers and mechanisms of tree mortality in moist tropical forests. *New Phytologist*, 219, 851–869. https://doi.org/10.1111/nph.15027

Mitchard, E. T. A. (2018). The tropical forest carbon cycle and climate change. *Nature*, 559, 527–534. https://doi.org/10.1038/s41586-018-0300-2

Nemani, R. R., Keeling, C. D., Hashimoto, H., Jolly, W. M., Piper, S. C., Tucker, C. J., ... Running, S. W. (2003). Climate-driven increases in global terrestrial net primary production from 1982 to 1999. *Science*, 300, 1560–1563. https://doi.org/10.1126/science.1082750

Pennekamp, F., Pontarp, M., Tabi, A., Altermatt, F., Alther, R., Choffat, Y., ... Petchey, O. L. (2018). Biodiversity increases and decreases ecosystem stability. *Nature*, 563, 109–112. https://doi.org/10.1038/s41586-018-0627-8

Phillips, O. L., Aragao, L. E. O. C., Lewis, S. L., Fisher, J. B., Lloyd, J., Lopez-Gonzalez, G., ... Torres-Lezama, A. (2009). Drought sensitivity of the Amazon rainforest. *Science*, 323, 1344–1347. https://doi.org/10.1126/science.1164033

Ponce-Campos, G. E., Moran, M. S., Huete, A., Zhang, Y., Bresloff, C., Huxman, T. E., ... Starks, P. J. (2013). Ecosystem resilience despite large-scale altered hydroclimatic conditions. *Nature*, 494, 349–352. https://doi.org/10.1038/nature11836

Poulter, B., Frank, D., Ciais, P., Myneni, R. B., Andela, N., Bi, J., ... van der Werf, G. R. (2014). Contribution of semi-arid ecosystems to inter-annual variability of the global carbon cycle. *Nature*, 509, 600–603. https://doi.org/10.1038/nature13376

Reichstein, M., Bahn, M., Ciais, P., Frank, D., Mahecha, M. D., Seneviratne, S. I., ... Wattenbach, M. (2013). Climate extremes and the carbon cycle. *Nature*, 500, 287–295. https://doi.org/10.1038/nature12350

Running, S. W. (2012). A measurable planetary boundary for the biosphere. *Science*, 337, 1458–1459. https://doi.org/10.1126/science.1227620

Saatchi, S., Asefi-Najafabady, S., Malhi, Y., Aragão, L. E. O. C., Anderson, L. O., Myneni, R. B., & Nemani, R. (2013). Persistent effects of a severe drought on Amazonian forest canopy. *Proceedings of the National Academy of Sciences of the United States of America*, 110, 565–570. https://doi.org/10.1073/pnas.1204651110

Saleska, S. R., Wu, J., Guan, K. Y., Araujo, A. C., Huete, A., Nobre, A. D., & Restrepo-Coupe, N. (2016). Dry-season greening of Amazon forests. *Nature*, 531, E4–E5. https://doi.org/10.1038/nature16457

Schewe, J., Gosling, S. N., Reyer, C., Zhao, F., Ciais, P., Elliott, J., ... Warszawski, L. (2019). State-of-the-art global models underestimate impacts from climate extremes. *Nature Communications*, 10, 1005. https://doi.org/10.1038/S41467-019-08745-6

Schwalm, C. R., Anderegg, W. R. L., Michalak, A. M., Fisher, J. B., Biondi, F., Koch, G., … Tian, H. (2017). Global patterns of drought recovery. *Nature*, *548*, 202–205. https://doi.org/10.1038/nature23021

Seddon, A. W. R., Macias-Faria, M., Long, P. R., Benz, D., & Willis, K. J. (2016). Sensitivity of global terrestrial ecosystems to climate variability. *Nature*, *531*, 229–232. https://doi.org/10.1038/nature16986

Sen, P. K. (1968). Estimates of the regression coefficient based on Kendall's Tau. *Journal of the American Statistical Association*, *63*, 1379–1389. https://doi.org/10.1080/01621459.1968.10480934

Sheffield, J., Goteti, G., & Wood, E. F. (2006). Development of a 50-year high-resolution global dataset of meteorological forcings for land surface modeling. *Journal of Climate*, *19*, 3088–3111. https://doi.org/10.1175/Jcli3790.1

Shi, Z., Xu, X., Souza, L., Wilcox, K., Jiang, L., Liang, J., … Luo, Y. (2016). Dual mechanisms regulate ecosystem stability under decade-long warming and hay harvest. *Nature Communications*, *7*, 11973. https://doi.org/10.1038/ncomms11973

Sippel, S., Reichstein, M., Ma, X., Mahecha, M. D., Lange, H., Flach, M., & Frank, D. (2018). Drought, heat, and the carbon cycle: A review. *Current Climate Change Reports*, *4*, 266–286. https://doi.org/10.1007/s40641-018-0103-4

Sitch, S., Huntingford, C., Gedney, N., Levy, P. E., Lomas, M., Piao, S. L., … Woodward, F. I. (2008). Evaluation of the terrestrial carbon cycle, future plant geography and climate-carbon cycle feedbacks using five Dynamic Global Vegetation Models (DGVMs). *Global Change Biology*, *14*, 2015–2039. https://doi.org/10.1111/j.1365-2486.2008.01626.x

Tang, H., & Dubayah, R. (2017). Light-driven growth in Amazon evergreen forests explained by seasonal variations of vertical canopy structure. *Proceedings of the National Academy of Sciences of the United States of America*, *114*, 2640–2644. https://doi.org/10.1073/pnas.1616943114

Tilman, D., & Downing, J. A. (1994). Biodiversity and stability in grasslands. *Nature*, *367*, 363–365. https://doi.org/10.1038/367363a0

Tilman, D., Reich, P. B., & Knops, J. M. H. (2006). Biodiversity and ecosystem stability in a decade-long grassland experiment. *Nature*, *441*, 629–632. https://doi.org/10.1038/nature04742

Van Ruijven, J., & Berendse, F. (2010). Diversity enhances community recovery, but not resistance, after drought. *Journal of Ecology*, *98*, 81–86. https://doi.org/10.1111/j.1365-2745.2009.01603.x

Vicente-Serrano, S. M. (2006). Differences in spatial patterns of drought on different time scales: An analysis of the Iberian Peninsula. *Water Resources Management*, *20*, 37–60. https://doi.org/10.1007/s11269-006-2974-8

Vicente-Serrano, S. M., Beguería, S., & López-Moreno, J. I. (2009). A multiscalar drought index sensitive to global warming: The standardized precipitation evapotranspiration index. *Journal of Climate*, *23*, 1696–1718. https://doi.org/10.1175/2009jcli2909.1

Vicente-Serrano, S. M., Gouveia, C., Camarero, J. J., Beguería, S., Trigo, R., Lopez-Moreno, J. I., … Sanchez-Lorenzo, A. (2013). Response of vegetation to drought time-scales across global land biomes. *Proceedings of the National Academy of Sciences of the United States of America*, *110*, 52–57. https://doi.org/10.1073/pnas.1207068110

Wagner, F. H., Hérault, B., Rossi, V., Hilker, T., Maeda, E. E., Sanchez, A., … Aragão, L. E. O. C. (2017). Climate drivers of the Amazon forest greening. *PLoS ONE*, *12*, e0180932. https://doi.org/10.1371/journal.pone.0180932

Wang, W., Wang, J., Liu, X., Zhou, G., & Yan, J. (2016). Decadal drought deaccelerated the increasing trend of annual net primary production in tropical or subtropical forests in southern China. *Scientific Report*, *6*, 28640. https://doi.org/10.1038/srep28640

Way, D. A. (2019). Just the right temperature. *Nature Ecology & Evolution*, *3*, 718–719. https://doi.org/10.1038/s41559-019-0877-3

Wei, S. H., Yi, C. X., Fang, W., & Hendrey, G. (2017). A global study of GPP focusing on light-use efficiency in a random forest regression model. *Ecosphere*, *8*, e01724. https://doi.org/10.1002/ecs2.1724

Wu, J., Albert, L. P., Lopes, A. P., Restrepo-Coupe, N., Hayek, M., Wiedemann, K. T., … Saleska, S. R. (2016). Leaf development and demography explain photosynthetic seasonality in Amazon evergreen forests. *Science*, *351*, 972–976. https://doi.org/10.1126/science.aad5068

Wu, J., Guan, K., Hayek, M., Restrepo-Coupe, N., Wiedemann, K. T., Xu, X., … Saleska, S. R. (2017). Partitioning controls on Amazon forest photosynthesis between environmental and biotic factors at hourly to interannual timescales. *Global Change Biology*, *23*, 1240–1257. https://doi.org/10.1111/gcb.13509

Xu, X. T., Medvigy, D., Powers, J. S., Becknell, J. M., & Guan, K. Y. (2016). Diversity in plant hydraulic traits explains seasonal and inter-annual variations of vegetation dynamics in seasonally dry tropical forests. *New Phytologist*, *212*, 80–95. https://doi.org/10.1111/nph.14009

Zeng, N., Zhao, F., Collatz, G. J., Kalnay, E., Salawitch, R. J., West, T. O., & Guanter, L. (2014). Agricultural Green Revolution as a driver of increasing atmospheric CO_2 seasonal amplitude. *Nature*, *515*, 394–397. https://doi.org/10.1038/nature13893

Zhou, G., Wei, X., Wu, Y., Liu, S., Huang, Y., Yan, J., … Liu, X. (2011). Quantifying the hydrological responses to climate change in an intact forested small watershed in Southern China. *Global Change Biology*, *17*, 3736–3746. https://doi.org/10.1111/j.1365-2486.2011.02499.x

Zhou, L., Tian, Y., Myneni, R. B., Ciais, P., Saatchi, S., Liu, Y. Y., … Hwang, T. (2014). Widespread decline of Congo rainforest greenness in the past decade. *Nature*, *509*, 86–90. https://doi.org/10.1038/nature13265

Zscheischler, J., Mahecha, M. D., von Buttlar, J., Harmeling, S., Jung, M., Rammig, A., … Reichstein, M. (2014). A few extreme events dominate global interannual variability in gross primary production. *Environmental Research Letters*, *9*, 035001. https://doi.org/10.1088/1748-9326/9/3/035001

SUPPORTING INFORMATION

Additional supporting information may be found online in the Supporting Information section at the end of the article.